Actuation of synthetic cells with proton gradients generated by light-harvesting E. coli

Kevin Jahnke
Max Planck Institute for Medical Research
Noah Ritzmann
Eidgenössische Technische Hochschule (ETH) Zurich
Julius Fichtler
Max Planck Institute for Medical Research
Anna Nitschke
Max Planck Institute for Medical Research
Yannik Dreher
Max Planck Institute for Medical Research
Tobias Abele
Max Planck Institute for Medical Research
Götz Hofhaus
Centre for Advanced Materials, Heidelberg University
Ilia Platzman
Max Planck Institute for Medical Research
Rasmus Schröder
Heidelberg University
Daniel Muller
Swiss Federal Institute of Technology in Zurich https://orcid.org/0000-0003-3075-0665
Joachim Spatz
Max Planck Institute for Medical Research
Kerstin Göpfrich (kerstin.goepfrich@mr.mpg.de)
Max Planck Institute for Medical Research https://orcid.org/0000-0003-2115-3551

Article

Keywords: synthetic biology, E. coli, proton gradient

Posted Date: November 6th, 2020

DOI: https://doi.org/10.21203/rs.3.rs-82114/v1

Version of Record: A version of this preprint was published at Nature Communications on June 25th, 2021. See the published version at https://doi.org/10.1038/s41467-021-24103-x.

Actuation of synthetic cells with proton gradients generated by light-harvesting E. coli

Kevin Jahnke,[†,‡] Noah Ritzmann,[¶] Julius Fichtler,[†] Anna Nitschke,[§] Yannik Dreher,[†,‡] Tobias Abele,[†,‡] Götz Hofhaus,[‖] Ilia Platzman,[§,⊥] Rasmus Schröder,[‖] Daniel J. Müller,[¶] Joachim P. Spatz,[§,⊥,#] and Kerstin Göpfrich[*,†,‡]

†*Max Planck Institute for Medical Research, Biophysical Engineering Group, Jahnstraße 29, 69120 Heidelberg, Germany*

‡*Department of Physics and Astronomy, Heidelberg University, 69120 Heidelberg, Germany*

¶*Department of Biosystems Science and Engineering, Eidgenössische Technische Hochschule (ETH) Zurich, Mattenstraße 26, 4058 Basel, Switzerland*

§*Max Planck Institute for Medical Research, Department of Cellular Biophysics, Jahnstraße 29, 69120 Heidelberg, Germany*

‖*Centre for Advanced Materials, Im Neuenheimer Feld 267, 69120 Heidelberg, Germany*

⊥*Institute for Molecular Systems Engineering (IMSE), Heidelberg University, Im Neuenheimer Feld 225, 69120 Heidelberg, Germany*

#*Max Planck School Matter to Life, Jahnstraße 29, 69120 Heidelberg, Germany*

E-mail: kerstin.goepfrich@mr.mpg.de

Abstract

Bottom-up and top-down approaches to synthetic biology each employ distinct methodologies with the common aim to harness new types of living systems. Both approaches, however, face their own challenges towards biotechnological and biomedical applications. Here, we realize a strategic merger to convert light into proton gradients for the actuation of synthetic cellular systems. We genetically engineer *E. coli* to overexpress the light-driven inward-directed proton pump xenorhodopsin and encapsulate them as organelle mimics in artificial cell-sized compartments. Exposing the compartments to light-dark cycles, we can reversibly switch the pH by almost one pH unit and employ these pH gradients to trigger the attachment of DNA structures to the compartment periphery. For this purpose, a DNA triplex motif serves as a nanomechanical switch responding to the pH-trigger of the *E. coli*. By attaching a polymerized DNA origami plate to the DNA triplex motif, we obtain a cytoskeleton mimic that considerably deforms lipid vesicles in a pH-responsive manner. We foresee that the combination of bottom-up and top down approaches is an efficient way to engineer synthetic cells as potent microreactors.

Main

Synthetic biology cultivates an engineering approach to biology with the aim to create or to re-purpose biological parts for specific tasks. The field is commonly divided into two branches with distinct tools and methodologies, but also distinct challenges – top-down and bottom-up synthetic biology.[1,2] The top-down approach uses genetic engineering techniques to manipulate natural cells, reprogramming their behavior and equipping them with new and exciting functions.[3] *Escherichia coli* bacteria, for instance, have been engineered for a variety of tasks, including biofuel production,[4] cancer cell targeting[5] or light harvesting.[6,7] Yet living cells remain too complex to achieve full control and not all added functions are compatible with the host.[8]

The bottom-up approach, on the other hand, has been successful at reconstituting natural biomolecules, or artificial components in cell-sized confinement like microfluidic droplets or lipid vesicles.[9–11] Noteworthy modules have been implemented so far, each mimicking a specific function of a living cell, including energy generation,[12,13] metabolism,[14] motility,[15,16] cytoskeletal contraction[17] or division.[18] Yet the combination of these modules towards complex signaling pathways for dynamic systems remains challenging.

Merging the capacities of top-down and bottom-up approaches to synthetic biology can be a leap forward towards complex bottom-up assemblies but also more versatile and well-defined top-down systems. Leading to this direction, communication between natural and synthetic cells has been implemented[19–21] and bottom-up assembled vesicles were used as organelle mimics in living cells.[22] Furthermore, engineered prokaryotes have recently been used as artificial organelles in living cells,[23,24] yet this has never been translated into synthetic cells. Here, we use top-down genetic engineering to equip *E. coli* with light-harvesting capabilities. We employ them as synthetic organelle mimics inside bottom-up assembled synthetic cellular compartments. Thereby, we can reversibly switch the pH upon illumination to trigger an optical or a nanomechanical response. The latter is based on the pH-sensitive membrane attachment of a triplex-forming DNA motif. Furthermore, we sculpt the synthetic cellular compartments in a pH-dependent manner by attaching a DNA origami plate to the pH-sensitive DNA strand.

Results

Top-down engineering of *E. coli* for light-harvesting

To equip synthetic cells with the capability to generate proton gradients, we set out to assemble an energy module. We genetically engineered *E. coli* to overexpress the light-driven proton pump xenorhodopsin, a transmembrane protein from nanohalosarchaeon *Nanosalina*.[25] It contains a retinal which, upon illumination, undergoes a trans-cis conformational

change and shuttles a proton across the lipid membrane. We chose xenorhodopsin because it shows unique features compared to other proton pumps, such as bacteriorhodopsin or proteorhodopsin: First of all, xenorhodopsin exhibits a substantially faster photocycle, which can result in larger proton gradients.[25] Secondly, as an inward-directed pump,[26] xenorhodopsin increases the pH (instead of decreasing it) in the extracellular space upon illumination (Figure 1a). As an additional feature, we introduced a C-terminal fluorescent GFP or mCherry tag to xenorhodopsin for vizualization of the *E. coli*. The choice of two dyes allows us to work with different combinations of fluorophores as required.

To assess and quantify the proton pumping capabilities of the genetically engineered *E. coli*, we performed a photoactivity assay, where we inserted a micro pH electrode into the *E. coli* suspension and exposed it to multiple light-dark cycles. Illumination increased the pH in the extracellular space by almost one pH unit within five minutes (Figure 1b), because protons are translocated from the extracellular solution to the cytosol. Longer illumination times resulted in saturation of the pH change (Supplementary Figure S1). The pH quickly returned to its initial value after the light was turned off due to the dissipation of protons. Even after three complete light-dark cycles, we observed only little decrease in the pH gradient. Compared to previous reports where proton pumps were reconstituted in lipid vesicles,[7,27] we could achieve faster and higher pH gradients using genetically engineered *E. coli*. Moreover, the use of *E. coli* circumvented the need for cumbersome protein purification and reconstitution to prepare proteoliposomes,[28] which highlights a key advantage of merging top-down and bottom-up synthetic biology.

As a next step, we aimed to encapsulate the *E. coli* as a pH switch in synthetic cells, which makes pH monitoring with an electrode impractical. We thus supplement the *E. coli* suspension with the ratiometric pH-sensitive fluorescent dye pyranine. The fluorescence properties of pyranine depend on its protonation state (Figure 1c, Supplementary Figure S2). After suitable calibration measurements (Supplementary Figure S3), we could hence monitor the pH optically.[29] Figure 1d plots the fluorescence intensity ratio over time while the system

was exposed to light-dark cycles (Supplementary Video S1, Figure S4). Notably, we obtained the same results as previously with the pH electrode.

Genetically engineered *E. coli* as synthetic organelles

Having demonstrated light-activated pH switching in bulk, we wanted to integrate the engineered *E. coli* as artificial mitochondria mimics in synthetic cell-sized confinements. Using a microfluidic droplet formation device (Figure 2a), *E. coli* and pyranine were encapsulated in surfactant-stabilized water-in-oil droplets (Figure 2b; Supplementary Figure S5). We obtained homogeneous compartments with a radius of $27\pm5\,\mu$m (mean±s.d., n=53) and a uniform distribution of *E. coli* (Figure 2c). Pyranine served as a fluorescent pH indicator inside the compartments (Figure 2d; Supplementary Figure S6). We exposed the system to three consecutive light-dark cycles. Illumination with white light triggered a pH increase inside the cell-sized compartments due to the light-driven proton transport by the *E. coli*, resulting in an optical response of the compartments themselves (Figure 2e; Supplementary Video S2). Taken together, we demonstrated that the genetically engineered *E. coli* can provide light-activated proton gradients in cell-sized compartments.

pH-sensitive attachment of DNA to the compartment periphery

Proton gradients in synthetic systems are especially exciting if they can be utilized to control and energize downstream processes. Instead of relying on purified proteins, an increasingly popular approach is to construct such pH-dependent machineries *de novo* from molecular building blocks. DNA nanotechnology, in particular, has been employed to build a variety of functional components for synthetic cells,[17,30,31] including membrane-sculpting[32–35] and pH-responsive components such as filaments[36] or rotors.[37,38] However, pH-responsive actuation is challenging after encapsulation into a compartment. With the *E. coli*, we can circumvent this by converting light into a proton gradient.

Towards this goal, we want to implement pH-induced membrane modification and remod-

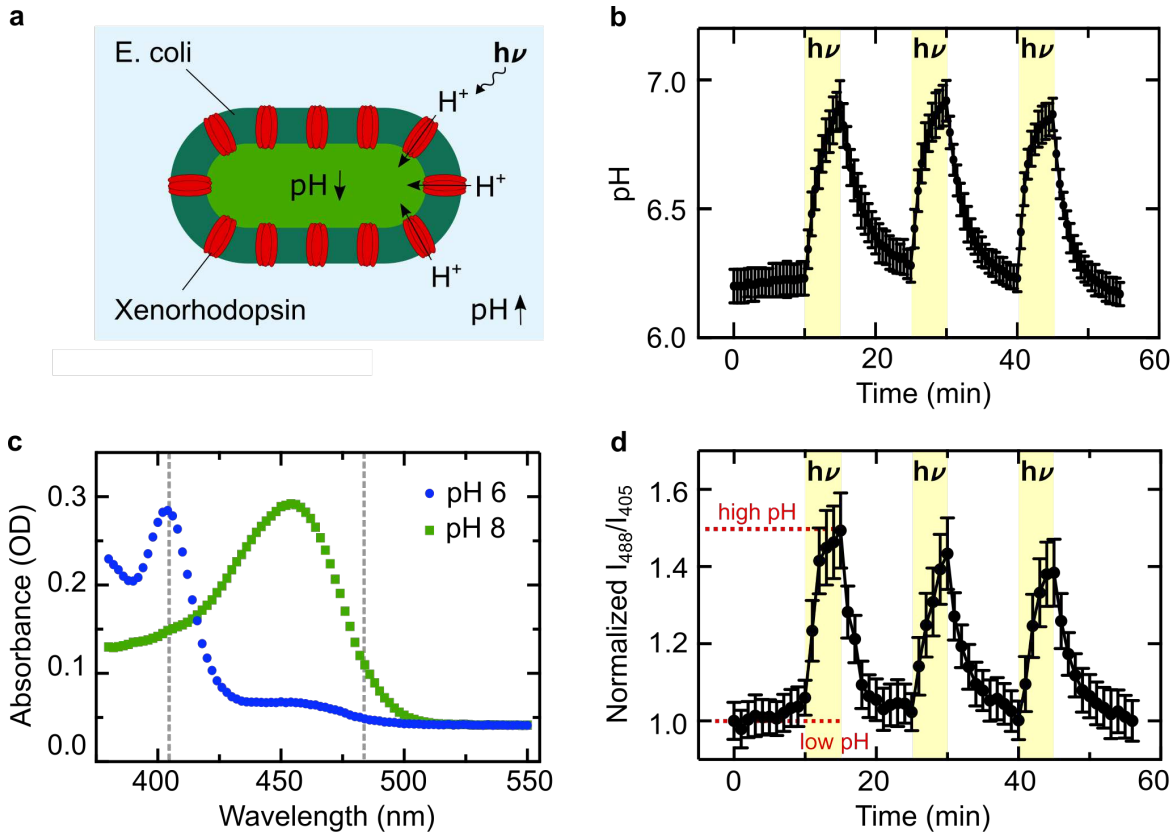

Figure 1: Genetically engineered xenorhodopsin-expressing *E. coli* generate a pH gradient upon illumination with white light. **a** Schematic illustration of an *E. coli* expressing xenorhodopsin, a light-driven proton pump (red), allowing for the reversible generation of a directional pH gradient during illumination with white light. The inward pump increases the pH of the external solution. **b** Photoactivity generated by the *E. coli* (OD_{600}=20, in 150 mM NaCl) measured with an external pH electrode. The pH is plotted over time during three light-dark cycles (periods of illumination are indicated in yellow). The pH increases by almost one pH unit within 5 min of illumination and nearly returns to its original value after 10 min in the dark (mean±s.d., n=3). **c** Absorbance measurements of the pH-sensitive ratiometric fluorophore pyranine at pH 6 (blue) and pH 8 (green). The pH can be quantified as the fluorescence intensity ratio at the excitation wavelengths 488 nm and 405 nm (gray dashed lines). **d** Normalized fluorescence intensity ratio I_{488}/I_{405} of pyranine (50 µM) over time in a solution containing *E. coli* and lipid vesicles as determined with confocal fluorescence microscopy (mean±s.d., n=4). Periods of illumination are indicated in yellow.

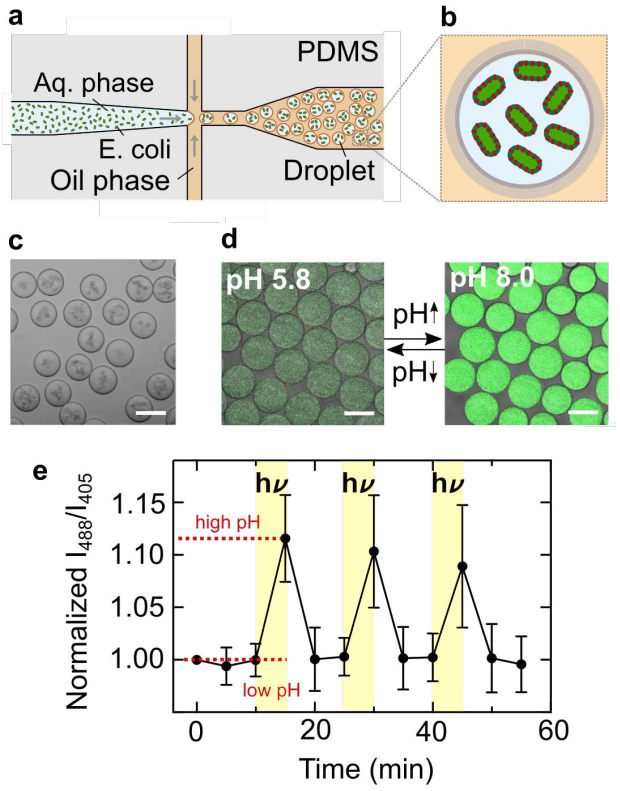

Figure 2: Using *E. coli* as light-activated synthetic organelles that change the pH inside cell-sized confinement. **a** Schematic illustration of the microfluidic device used to encapsulate engineered *E. coli* and pyranine into cell-sized compartments. Water-in-oil droplets were generated at a flow-focusing T-junction of a PDMS-based device. **b** Schematic illustration of a surfactant-stabilized water-in-oil droplet containing engineered *E. coli*. **c** Brightfield image of monodisperse water-in-oil droplets with a radius of 27±5 μm (mean±s.d., n=53) containing engineered *E. coli* (OD_{600} = 20). Scale bar: 50 µm. **d** Overlay of confocal fluorescence and brightfield images of pyranine (c= 50 µM, λ_{ex}=488 nm) inside droplet-based compartments at pH 5.8 and pH 8.0. Scale bar: 50 µm. **e** Normalized fluorescence intensity ratio I_{488}/I_{405} of *E. coli* and pyranine-containing droplets over time. The fluorescence intensity ratio (mean±s.d., n=11 droplets) of pyranine (and hence the pH) increases reversibly during periods of illumination with white light (30 W halogen bulb, highlighted in yellow). Note that the number of recorded frames was reduced because the illumination light had to be turned off each time an image was acquired, which will bias the proton pumping activity.

eling. For this purpose, we employ a single-stranded DNA sequence, which consists of specifically designed sections:[36] First, it contains a self-complementary section, which forms a DNA duplex following the Watson-Crick basepairing rules. A single-stranded hairpin loop connects the duplex-forming sections. Another critical single-stranded region is located at the 3' end. At acidic pH it wraps around the DNA duplex to form a triplex, held together by Hoogsten interactions. At basic pH, the triplex becomes unstable. The remaining duplex can now also open up, if a second DNA strand with higher affinity binds to the hairpin loop.[36] By functionalizing this second DNA strand with a terminal cholesterol tag, it self-assembles at the compartment periphery due to hydrophobic interactions.[39] Thereby, we can recruit the triplex-motif strand to the compartment-periphery in a pH-reversible manner (Figure 3a). At basic pH, the triplex-motif strand is bound to the periphery (Figure 3b, inset top right and Supplementary Figure S7). At acidic pH, on the other hand, it remains homogeneously distributed inside the compartment (Figure 3b, inset bottom left). To characterize the pH-sensitive membrane attachment, we assessed the fluorescence intensity inside the compartment as a function of pH. The fluorescence intensity decrease with increasing pH follows a sigmoidal fit with a turning point at pH 6.05, which is compatible with the pH range of the *E. coli*.

As a next step, we need to verify that membrane attachment of the DNA can also be triggered by the engineered *E. coli*. We hence co-encapsulated them with the cholesterol-tagged as well as the triplex-forming DNA strand using a microfluidic two-inlet device (Supplementary Figure S5). A second inlet proved to be advantageous, because the cholesterol-tagged DNA could bind to the droplet periphery before encountering the *E. coli*, hence preventing unwanted attachment to the *E. coli* due to hydrophobic interactions.[40]

After microfluidic droplet formation in the dark, the triplex-forming DNA was homogeneously distributed inside the compartment with some attachment to the periphery (Figure 3c). From the calibration curve, we could deduce a starting pH value of around 6.0-6.5, consistent with previous experiments. Upon illumination, the DNA attached to the com-

partment periphery over the course of 30 minutes (Figure 4d, Supplementary Video S4). We obtained a pH increase of almost one pH unit, consistent with the bulk experiments in Figure 1. The dynamic opening of the triplex and subsequent attachment to the periphery was considerably slower than the pyranine response.[36] We observed that the DNA remained attached to the compartment periphery after the light was turned off. We found that this is due to an interesting hysteresis effect: Once the DNA duplex at the droplet periphery was formed, the detachment of the triplex-forming DNA was shifted to substantially lower pH values (Supplementary Figure S8). Therefore, the DNA did not detach when the pH returned to its original value after turning off the light. Detachment could, however, be achieved with larger pH gradients: Figure 3e shows the reversible attachment of the DNA triplex to the compartment periphery, triggered by the addition of a proton acceptor (1 vol% propylamine in HFE) and subsequent addition of a proton donor (1 vol% trifluoroacetic acid in HFE).

We have thus realized a complex reaction pathway, where illumination activates the internal organelle mimics, causing a proton gradient which, in turn, leads to the stable modification of the compartment periphery. Moreover, the pH-sensitive membrane attachment and the discovered hysteresis effect extend the scope of the DNA triplex motif in DNA nanotechnology.

pH-induced morphology change

Finally, we can exploit the pH-responsive modification of the compartment periphery to provide a meaningful function. Assuming that the DNA triplex motif could serve as a shuttle to bring components to the periphery, we set out to develop a cytoskeleton mimic, which could sculpt synthetic cellular compartments in a pH-responsive manner. For this purpose, we designed a DNA origami plate made of two layers of DNA helices (Figure 4a, Supplementary Figure S9). The two layers were twisted at a 90° angle as visible in the cryo electron micrographs (Figure 4b), enabling blunt-end stacking[41] on all four sides of the DNA origami.

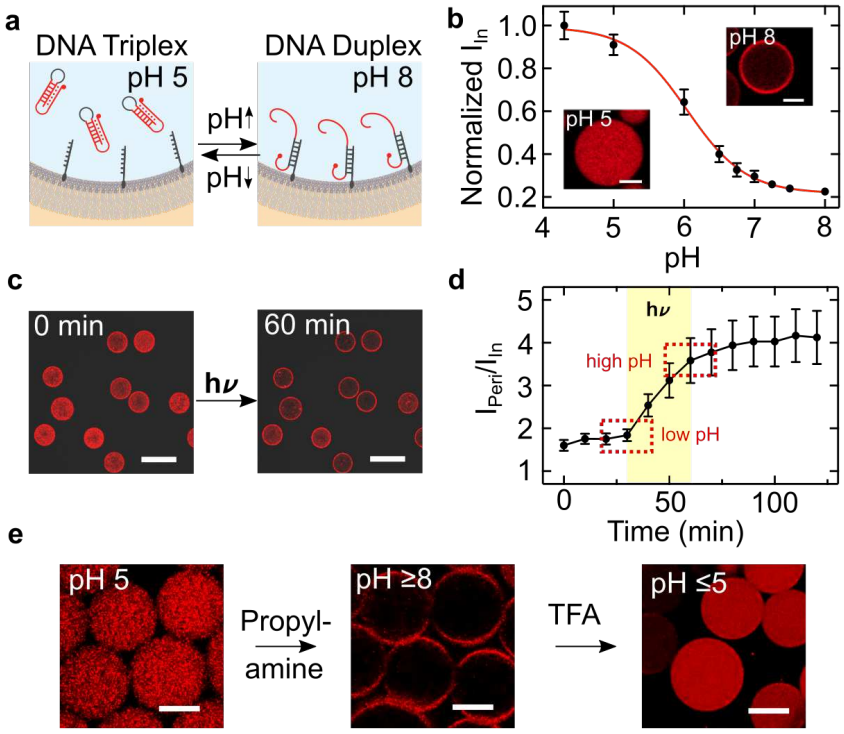

Figure 3: pH-sensitive DNA attachment to the droplet periphery stimulated with engineered *E. coli*. **a** Schematic illustration of pH-sensitive duplex formation at the droplet periphery. In response to higher pH, the DNA triplex motif opens up and reversibly attaches to the cholesterol-tagged DNA handles at the compartment periphery. **b** Normalized fluorescence intensity of triplex-forming DNA inside the droplet (excluding the periphery) dependent on the pH (mean±s.d., n=20). The sigmoidal fit (red curve) has a turning point at pH 6.05. The insets depict confocal fluorescence images of Cy5-labeled triplex-forming DNA (λ_{ex}=647 nm, 1 μM) inside a water-in-oil droplet (containing 1.5 μM cholesterol-tagged DNA) at pH 5 (bottom left) and pH 8 (top right). At pH 8, the triplex-forming DNA is located at the droplet periphery, whereas it is homogeneously distributed at pH 5. Scale bars: 20 µm. **c** Confocal images of microfluidic water-in-oil droplets containing the triplex-forming DNA (λ_{ex}=647 nm), cholesterol-tagged DNA and engineered *E. coli* before (0 min) and after (60 min) illumination with white light. Scale bars: 100 µm. **d** Fluorescence intensity ratio I_{peri}/I_{in} (mean±s.d., n=20) of the triplex-forming DNA over time. The ratio increases during light illumination due to binding of the triplex-forming DNA to the droplet periphery. The time period of illumination is indicated in yellow. **e** Confocal images of microfluidic water-in-oil droplets containing the triplex-forming DNA (λ_{ex}=647 nm) and cholesterol-tagged DNA produced at pH 5 (left image). Flushing of the proton acceptor propylamine (1 vol% in HFE) led to a pH increase of the aqueous solution inside the droplets and hence attachment of the triplex-forming DNA (middle). Subsequent flushing of the proton donor trifluoroacetic acid (1 vol% in HFE) decreased the pH and hence causes DNA detachment (right). The attachment of triplex-forming DNA to the droplet periphery is reversible. Scale bars: 30 µm.

This, in turn, leads to efficient polymerization of the DNA origami monomers into large flat sheets (Supplementary Figure S10). The bottom-side of the DNA origami was functionalized with the DNA triplex motif at four positions. At basic pH, the DNA origami thus attached to the periphery of cell-sized droplets functionalized with the complementary cholesterol-tagged strand. However, the droplets remained spherical (Supplementary Figure S11). This is not surprising given that droplets could also not be deformed with cytoskeletal proteins due to their interfacial properties.[17,42] We thus moved to a compartment system which better mimics the mechanical properties of cellular membranes. We produced giant unilamellar lipid vesicles (GUVs) and functionalized them externally with the cholesterol-tagged DNA (Figure 4c). The GUVs remained stable in the *E. coli* culture as shown in the confocal image in Figure 4d. Upon illumination, we observed the pH-sensitive attachment of the DNA triplex strand (Figure 4e; Supplementary Figure S12), proving that the pH-signal-transduction between the top-down and bottom-up assembled synthetic cells is also successful when the *E. coli* are used as external actuators.

Attaching the DNA origami to the triplex strand, we observed considerable deviations from the initially spherical shape of the GUV (Figure 4f). Large flat sections appeared on the GUV with kinks at the phase boundaries between the polymerized flat DNA sheets. In addition to the morphological change, we observe a suppression of membrane fluctuations (Supplementary Figure S13, Video S5), indicating a mechanical stabilization of the compartment[35,43] by the DNA-based cytoskeleton mimic. Both the morphological and the mechanical alterations are reversible: Addition of a base led to pH decrease and hence to the detachment of the DNA origami from the GUV membrane. Notably, the GUV returned to its initial spherical shape (Figure 4f). The histograms in Figure 4g quantify the pH-reversible morphology change of the GUVs, revealing lower and more broadly distributed circularities when the DNA origami was attached at high pH. Taken together, the self-assembly of nanoscopic pH-responsive building blocks could trigger the microscopic morphological remodelling of the shape of lipid-membrane-based synthetic cellular compartments. The resulting compartment

stabilization could be exploited for drug delivery applications.

Conclusion

In summary, we have shown that the use of top-down engineered bacteria can enhance bottom-up assembled synthetic cells. The light-induced proton gradients we achieve with xenorhodopsin-overexpressing *E. coli* are not only larger than what was previously achieved with purified and reconstituted proteins – we also circumvent the laborious processes involved in their preparation. Especially membrane proteins, which can provide transient or chemically storable forms of energy as well as signal transduction and molecular transport in living cells, can be challenging to purify. Therefore, we can exploit the engineered *E. coli* to drive sophisticated downstream dynamics in synthetic cells. In particular, we demonstrate the pH-sensitive attachment of a triplex-motif-carrying DNA strand to the compartment periphery upon illumination. By attaching a DNA origami to the triplex-motif and providing a complementary DNA handle at the compartment periphery, we change the shape of GUVs in a pH-dependent manner. The possibility to manipulate lipid membranes and not just the DNA nanostructures themselves broadens the scope of the popular DNA triplex-motif. For biotechnological applications, compartments that modify themselves as a response to environmental factors are highly desirable. More general, the integration of top-down engineered cells into bottom-up synthetic biology, bridging a decade-long divide, will provide the potential to realize diverse functions beyond light-harvesting. This provides a route to construct potent microreactors for biotechnology. Just like the endosymbiosis of free-living prokaryotes was a critical step in the evolution of eukaryotic cells, we envision that the integration of top-down engineered components in synthetic cells will be a leap forward in their complexity and functionality.

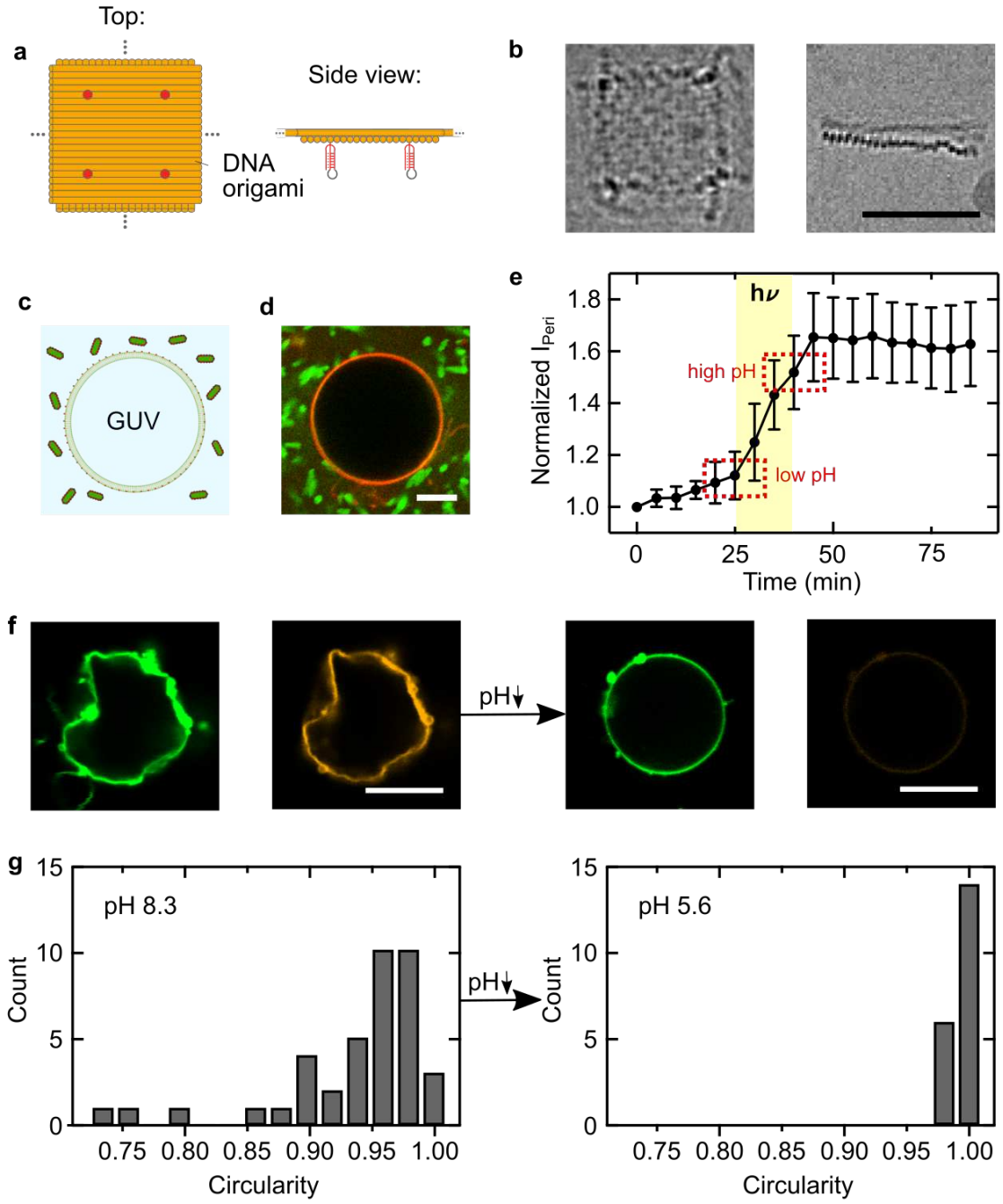

Figure 4: Deformation of GUVs with pH-sensitive DNA origami. **a** Schematic illustration of the DNA origami, which can polymerize into flat DNA origami sheets due to blunt end stacking. The DNA origami was functionalized with four DNA triplex motifs (red, two are shown), such that its assembly on the GUV membrane is pH-dependent.**b** Cryo-EM micrographs of the DNA origami plates. The top view (left) and the side view (right) showing the two DNA layers connected at a 90° angle. Scale bar: 50 nm. **c** Schematic illustration of a GUV immersed in a bath of engineered *E. coli*. (Continued on the following page)

Figure 4: (Continued) **d** Confocal image of a DNA-coated GUV surrounded by *E. coli* as described in **a** (0.4 μM triplex-forming DNA, λ_{ex}=561 nm; 0.6 μM cholesterol-tagged DNA). Scale bar: 10 µm. **e** Normalized fluorescence intensity I_{peri} (mean±s.d., n=15) of the triplex-forming DNA at the GUV periphery monitored over time. The time period of illumination is indicated in yellow, illumination leads to a pH increase and hence DNA attachment. **f** Confocal images of GUVs before (left) and after (right) decreasing the pH from pH 8.3 to pH 5.6 by addition of iso-osmotic potassium dihydrogenphosphate buffer. The GUV (lipids labelled with Atto488, λ_{ex}= 488 nm) is initially deformed due to the membrane-bound polymerized DNA origami (labelled with Cy3, λ_{ex}= 561 nm). The DNA origami detaches upon lowering the pH (the fluorescence from the detached DNA origami in the background is too weak to be visible). Scale bars: 10 µm. **g** Histograms of GUV circularity before (left) and after (right) lowering the pH. At pH 8.3, the mean circularity is 0.94 ± 0.06 (n=39) compared to 0.991 ± 0.004 (n=20) at pH 5.6, respectively.

Methods

Cloning

The plasmid pNR31 harboring the xenorhodopsin gene from Nanosalina (NsXeR) fused to the gene coding for superfolder-GFP (sf-GFP) was assembled by replacing the gene coding for proteorhodopsin in plasmid pNR03[7] with the NsXeR gene (Supplementary Table S1). Therefore, a codon-optimized NsXeR gene based on the amino-acid sequence[25] with a 5' NdeI and a 3' BamHI restriction site was synthesized by GenScript (https://www.genscript.com) and cloned into the pUC57 plasmid. Using these two restriction enzymes (New England Biolabs, Ipswich, MA), the NsXeR gene was then subcloned into the pNR03 plasmid. The plasmid pNR33 harboring the NsXeR gene fused to mCherry (Supplementary Table S1) was assembled in multiple steps. First the sf-GFP gene in pNR03 was replaced by the gene coding for mCherry. To that end, the mCherry gene was amplified from the pNR09 plasmid using primers 5'-GGC GGA TCC ATG CAT AGC AAG GGC GAG-3' and 5'-GCC AAG CTT CTT GTA CAG C-3' to introduce 5' BamHI and 3' HindIII restriction sites.[7] The resulting PCR-product was then cloned into plasmid pNR03 where it replaced the sf-GFP gene. Subsequently the same subcloning as for plasmid pNR31 was performed to replace the gene coding for proteorhodopsin with the NsXeR gene.

Overexpression of fusion-proteins in *E. coli*

E. coli C41 (DE3) cells (Sigma-Aldrich) were transformed with the plasmids pNR31 and pNR33. 100 mL Luria-Bertani liquid cultures (100 µg/mL ampicillin) were inoculated 1:100 from overnight cultures. The *E. coli* cells were grown at 37°C while shaking at 220 rpm until an OD600 of 0.4 was reached. Then, all-trans-retinal (Sigma-Aldrich) was added to a concentration of 10 µM and the expression of the fusion-proteins was induced with the addition of 1 mM isopropyl-D-thiogalactopyranoside (IPTG, Sigma-Aldrich). The cells were incubated for another 4 h at 37°C while shaking at 220 rpm. Subsequently they were harvested by centrifugation (3200 × g for 10 min at 4°C) and resuspended in 150 mM NaCl. The cells were stored at 4°C and protected from light until further use.

Photoactivity measurements with a micro pH-electrode

E. coli cells overexpressing either XeR-GFP or XeR-mCherry were washed twice with 150 mM NaCl (3200 × g for 10 min at 4 °C) prior to photoactivity measurements. Immediately before the measurement, another washing step was performed. The bacteria were concentrated to an OD_{600} of 20. Photoactivity measurements were conducted using a micro pH-electrode (InLab Micro Pro, Mettler Toledo, Columbus, OH) and a sample volume of 800 μL. The pH was recorded every 10 s. During the measurements the bacteria were protected from ambient light and continuously stirred to prevent sedimentation. The sample was illuminated for 5 min during each light-dark cycle. After each illumination-period the sample was kept in the dark for 10 min. All measurements were performed at room temperature.

Confocal fluorescence microscopy

A confocal laser scanning microscope LSM 880, LSM 800 or LSM 700 (Carl Zeiss AG) was used for confocal imaging. The pinhole aperture was set to one Airy Unit and experiments were performed at room temperature. The images were acquired using a 20x (Objective Plan-Apochromat 20x/0.8 M27, Carl Zeiss AG). Images were analyzed and processed with

ImageJ (NIH, brightness and contrast adjusted).

Formation of surfactant-stabilized water-in-oil droplets

As previously described,[39] microfluidic PDMS-based (Sylgard 184, Dow Corning) devices for the formation of water-in-oil droplets were produced and assembled. The device layouts of the single and double inlet devices are shown in the Supplementary Figure S5. For the oil-phase, 1.4 vol% of Perflouro-polyether-polyethylene glycol (PFPE-PEG) block-copolymer fluorosurfactants (PEG-based fluorosurfactant, Ran Biotechnologies, Inc.) dissolved in HFE-7500 oil (DuPont) was used. The aqueous phase contained the encapsulated content and was varied as described in the corresponding sections. The fluid pressures were controlled by an Elveflow microfluidic flow control system or syringe pumps (Harvard Apparatus). The fluids were injected into the channels with 1 ml syringes (Omnifix, B.Braun, Germany) connected by a cannula (Sterican®0.4 x 20 mm, BL/LB, B.Braun) as well as PTFE-tubing (0.4 x 0.9 mm, Bola). To observe the production process, an Axio Vert.A1 (Carl Zeiss AG) inverse microscope was used. As an alternative to the microfluidic formation of droplets, the aqueous phase was layered on top of the oil phase within an microtube (Eppendorf) and droplet formation was induced by manual shaking as described earlier.[44]

Photoactivity measurements in droplets

Photoactivity measurements in droplets were performed by encapsulating *E. coli* (OD600≈20) with pyranine (50 µM) into surfactant-stabilized droplets using the microfluidic device described above. The droplets were stored at 4 °C after formation to allow for equilibration of the pH inside the droplet. Subsequently, droplets were sealed in an observation chamber and observed with confocal fluorescence microscopy. After 10 min of imaging in the dark, the sample was illuminated for 5 min using a Photonic PL 1000 lamp (light intensity 8 Mlx using a 30 W halogen bulb). The lightguide was placed 5-10 cm above the sample. These cycles were repeated for 1 h.

pH-sensitive attachment of DNA to the droplet periphery

Cholesterol-tagged DNA (sequence: 5' (Cy3)-ACCAGACAATACCACACAATTTT-CholTEG 3', HPLC purified) and the Cy-5 labelled triplex-forming DNA (sequence: 5' Cy5-TTCTCTT CTCGTTTGCTCTTCTCTTGTGTGGTATTGTCTAAGAGAAGAG 3', adapted from Green et al.,[36] HPLC purified) were purchased from Biomers or Integrated DNA Technologies. Both DNA sequences were encapsulated in microfluidic droplets at a concentration of 1.5 µM and 1 µM, respectively. For the calibration measurement (Figure 3b), the aqueous solution inside the droplets additionally contained 50 mM potassium phosphate buffer at the respective pH. Propylamine (from Sigma Aldrich) and Trifluoracetic Acid (TFA, from Sigma Aldrich) were flushed to dynamically change the pH of the droplets' aqueous phase. For the co-encapsulation of the DNA together with the *E. coli* ($OD_{600}\approx20$), a two-inlet droplet formation device was used (see Supplementary Figure S5). As previously, droplets were sealed in an observation chamber for confocal fluorescence imaging experiments.

GUVs electroformation and DNA attachment

GUVs consisting of 99 % DOPC (1,2-dioleoyl-sn-glycero-3-phosphocholine, from Avanti Polar Lipids) and 1 % Atto488-DOPE (1,2-dioleoyl-sn-glycero-3-phosphoethanolamine-Atto488, from AttoTEC) in 120 mM sucrose were produced via electroformation using a Vesicle Prep Pro (Nanion) as described previously.[34] An AC-current with an amplitude of 3 V and a frequency of 5 Hz was applied for 2 h at 37°C. The cholesterol-tagged DNA and the triplex-forming DNA were added to the GUVs at a concentration of 0.6 µM and 0.4 µM, respectively, before the addition of the *E. coli* ($OD_{600}\approx20$), in an unbuffered solution containing 150 mM NaCl and 5 mM $MgCl_2$.

DNA origami design and assembly

DNA origami structures were adapted from an earlier design by Kopperger et al.[45] using the open-access software *cadnano*[46]. Several changes were introduced, in particular: 1)

Addition of nine DNA staple strand overhangs on the top layer, complementary to single stranded fluorescent Cy3-tagged DNA; 2) Addition of four single stranded overhangs on the bottom layer, complementary to the triplex-forming DNA; 3) Complete redesign of the edge staples resulting in a cross-shaped plate. The sticky cross DNA origami contained edge staples that finish the scaffold seam, enabling blunt-end stacking with neighbouring origami. 4) Use of the longer single-stranded scaffold DNA, type p8064. A complete list of the DNA sequences is shown in Tables S2 and S3, the details of the design are shown in Figure S10. DNA origami was assembled as described previously[45]. All un-modified staple strands (Integrated DNA Technologies, Inc., purification: standard desalting) were added in a 5-fold excess compared to the p8064 scaffold strand (tilibit nanosystems GmbH). The solution contained 1× TAE (Tris-Acetate-EDTA, Sigma-Aldrich), 20 mM $MgCl_2$ (Sigma-Aldrich), pH 7.4. The structures were annealed in a thermocycler (Bio-Rad T100) that controls a temperature ramp from 70 °C to 20 °C over 12 h and successively holds the temperature at 40 °C for at least 3 h. The unpurified samples were stored at 4 °C until further use.

Purification of the DNA origami

Prior to purification from excess staples, the DNA origami was mixed with 1 µM Cy3-tagged single-stranded DNA (Integrated DNA Technologies, Inc., DNA sequence: 5' Cy3-AAAAAAAAAAAAAAAAAAAA 3', purification: HPLC) as well as a pH-sensitive triplex-forming DNA motif (Integrated DNA Technologies, Inc., DNA sequence: 5' TTCTCTTCTC GTTTGCTCTTCTCTTGTGTGGTATTGTCTAAGAGAAGAGTTTGATGCATAGAAGG 3'). The DNA origami was then suspendend in 500 µL of 1× TAE, 5 mM $MgCl_2$ and purification was preformed as previously described[31] by spin filtration in a Biofuge Fresco microlitre centrifuge (Heraeus 75005521) using 100 kDa cutoff filters from Amicon (Amicon Ultra-15, PLHK Ultracel-PL Membran, UFC910008). After filtration, the $MgCl_2$ concentration was raised to 20 mM again. To measure the DNA origami concentration a NanoDrop ND-1000 Spectrophotometer (PEQLAB Biotechnologie GmbH) was used yielding 6.5 nM.

Cryo electron microscopy

3 µL of the assembled origamis in 10 mM sodium phosphate pH 8.3 containing 20 mM $MgCl_2$ were blotted for 5-10 s in a (Vitrobot Mark IV, Thermo Fischer) on Quantifoli 2/1 grids with zero blot force at 100% humidity. Plunge frozen samples were imaged in a Krios equipped with a K3 camera behind an energy filter at a pixel size of 0.137 nm. Images were taken by single particle program (EPU, Thermo Fischer) with a a total dose of 20 e/A2. Movies of 20 frames were corrected[47] then cropped, normalized, low-pass filtered (0.0625) and 4x binned.[48]

GUV deformation with pH-sensitive DNA origami

The DNA origami (in 1 x TAE, 20 mM $MgCl_2$) was incubated with cholesterol-tagged DNA at 50 nM for 25 minutes and immediately mixed with Atto488 labelled iso-osomotic (120 mOsmol) GUVs in a ratio of one to three. DNA origami-coated GUVs were imaged after 24 hours of incubation in the fridge. Subsequently, the GUVs were incubated for another 24 hours with 48 mM KH_2PO_4 buffer in order to detach the DNA origami from the GUV membrane.

Acknowledgement

K.J., R.S., J.P.S. and K.G. acknowledge funding from the Deutsche Forschungsgemeinschaft (DFG, German Research Foundation) under Germany's Excellence Strategy via the Excellence Cluster 3D Matter Made to Order (EXC-2082/1 – 390761711). K.J. thanks the Carl Zeiss Foundation. J.P.S and I.P. acknowledge funding from the European Research Council, Grant Agreement no. 294852, SynAd, the MaxSynBio Consortium (jointly funded by the Federal Ministry of Education and Research of Germany and the Max Planck Society), from the SFB 1129 of the German Science Foundation and from the VolkswagenStiftung (priority call 'Life?'). J.P.S. is the Weston Visiting Professor at the Weizmann Institute of Science.

G.H. and R.S. acknowledge the services SDShd and bwHPC supported by the Ministry of Science, Research and the Arts Baden-Württemberg. The Krios microscope is part of the Cluster of Excellence "CellNetworks" (Exc 81) at the Universität Heidelberg. K.G. received funding from the European Union Horizon 2020 research and innovation program under the Marie Skłodowska-Curie grant agreement No. 792270. The authors acknowledge the Max Planck Society for its general support. N.R. and D.J.M. thank the Swiss Nanoscience Institute (SNI, Basel, Switzerland), the Swiss National Science Foundation and NCCR Molecular Systems Engineering for their support.

Supporting Information Available

Author contribution

K.J. performed most experiments and analysis. N.R. designed and prepared genetically engineered *E. coli* and performed pH electrode measurements. J.F. and K.G. designed the DNA origami. J.F. and K.J. carried out pH-sensitive deformation experiments. A.N. and K.J. established the use of pyranine as pH-sensor within droplets or GUVs. Y.D. and K.J. performed and analyzed pH-sensitive DNA attachment to GUVs. T.A. helped in analyzing the fluorescence ratios. G.H. and R.S. designed and carried out cryo-EM experiments. K.J., K.G., I.P., D.J.M. and J.P.S. designed the study. K.J. and K.G. wrote the manuscript with help from all authors.

Competing interests

The authors declare no competing interests.

References

(1) Benner, S. A.; Sismour, A. M. Synthetic biology. *Nature Reviews Genetics* **2005**, *6*, 533–543.

(2) Schwille, P. Jump-starting life? Fundamental aspects of synthetic biology. *Journal of Cell Biology* **2015**, *210*, 687–690.

(3) Cameron, D. E.; Bashor, C. J.; Collins, J. J. A brief history of synthetic biology. *Nature Reviews Microbiology* **2014**, *12*, 381–390.

(4) Zhang, F.; Carothers, J. M.; Keasling, J. D. Design of a dynamic sensor-regulator system for production of chemicals and fuels derived from fatty acids. *Nature Biotechnology* **2012**, *30*, 354–359.

(5) Anderson, J.; Clarke, E.; Arkin, A.; Voigt, C. Environmentally Controlled Invasion of Cancer Cells by Engineered Bacteria. *Journal of molecular biology* **2006**, *355*, 619–27.

(6) Schuergers, N.; Werlang, C.; Boghossian, A. A. A Synthetic Biology Approach to Engineering Living Photovoltaics. *Energy & Environmental Science* **2017**, *10*, 1102–1115.

(7) Ritzmann, N.; Thoma, J.; Hirschi, S.; Kalbermatter, D.; Fotiadis, D.; Müller, D. J. Fusion Domains Guide the Oriented Insertion of Light-Driven Proton Pumps into Liposomes. *Biophysical Journal* **2017**, *113*, 1–6.

(8) Ausländer, S.; Ausländer, D.; Fussenegger, M. Synthetic Biology-The Synthesis of Biology. *Angewandte Chemie International Edition* **2017**, *56*, 6396–6419.

(9) Göpfrich, K.; Platzman, I.; Spatz, J. P. Mastering Complexity: Towards Bottom-up Construction of Multifunctional Eukaryotic Synthetic Cells. *Trends in Biotechnology* **2018**, *36*, 938–951.

(10) Schwille, P. et al. MaxSynBio: Avenues Towards Creating Cells from the Bottom Up. *Angewandte Chemie International Edition* **2018**, *57*, 13382–13392.

(11) Supramaniam,; Ces,; Salehi-Reyhani, Microfluidics for Artificial Life: Techniques for Bottom-Up Synthetic Biology. *Micromachines* **2019**, *10*, 299.

(12) Otrin, L.; Marušič, N.; Bednarz, C.; Vidaković-Koch, T.; Lieberwirth, I.; Landfester, K.; Sundmacher, K. Toward Artificial Mitochondrion: Mimicking Oxidative Phosphorylation in Polymer and Hybrid Membranes. *Nano Letters* **2017**, *17*, 6816–6821.

(13) Berhanu, S.; Ueda, T.; Kuruma, Y. Artificial photosynthetic cell producing energy for protein synthesis. *Nature Communications* **2019**, *10*, 1325.

(14) Miller, T. E.; Beneyton, T.; Schwander, T.; Diehl, C.; Girault, M.; McLean, R.; Chotel, T.; Claus, P.; Cortina, N. S.; Baret, J.-C.; Erb, T. J. Light-powered CO2 fixation in a chloroplast mimic with natural and synthetic parts. *Science* **2020**, *368*, 649–654.

(15) Keber, F. C.; Loiseau, E.; Sanchez, T.; DeCamp, S. J.; Giomi, L.; Bowick, M. J.; Marchetti, M. C.; Dogic, Z.; Bausch, A. R. Topology and dynamics of active nematic vesicles. *Science* **2014**, *345*, 1135–1139.

(16) Bartelt, S. M.; Steinkühler, J.; Dimova, R.; Wegner, S. V. Light-Guided Motility of a Minimal Synthetic Cell. *Nano Letters* **2018**, *18*, 7268–7274.

(17) Jahnke, K.; Weiss, M.; Weber, C.; Platzman, I.; Göpfrich, K.; Spatz, J. P. Engineering Light-Responsive Contractile Actomyosin Networks with DNA Nanotechnology. *Advanced Biosystems* **2020**, 2000102.

(18) Steinkühler, J.; Knorr, R. L.; Zhao, Z.; Bhatia, T.; Bartelt, S. M.; Wegner, S.; Dimova, R.; Lipowsky, R. Controlled division of cell-sized vesicles by low densities of membrane-bound proteins. *Nature Communications* **2020**, *11*, 1–11.

(19) Schwarz-Schilling, M.; Aufinger, L.; Mückl, A.; Simmel, F. C. Chemical communication between bacteria and cell-free gene expression systems within linear chains of emulsion droplets. *Integrative Biology* **2016**, *8*, 564–570.

(20) Lentini, R.; Martín, N. Y.; Forlin, M.; Belmonte, L.; Fontana, J.; Cornella, M.; Martini, L.; Tamburini, S.; Bentley, W. E.; Jousson, O.; Mansy, S. S. Two-Way Chemical Communication between Artificial and Natural Cells. *ACS Central Science* **2017**, *3*, 117–123.

(21) Lentini, R.; Santero, S. P.; Chizzolini, F.; Cecchi, D.; Fontana, J.; Marchioretto, M.; Del Bianco, C.; Terrell, J. L.; Spencer, A. C.; Martini, L.; Forlin, M.; Assfalg, M.; Serra, M. D.; Bentley, W. E.; Mansy, S. S. Integrating artificial with natural cells to translate chemical messages that direct E. coli behaviour. *Nature Communications* **2014**, *5*, 1–6.

(22) Staufer, O.; Schröter, M.; Platzman, I.; Spatz, J. P. Bottom-Up Assembly of Functional Intracellular Synthetic Organelles by Droplet-Based Microfluidics. *Small* **2020**, *1906424*.

(23) Mehta, A. P.; Supekova, L.; Chen, J. H.; Pestonjamasp, K.; Webster, P.; Ko, Y.; Henderson, S. C.; McDermott, G.; Supek, F.; Schultz, P. G. Engineering yeast endosymbionts as a step toward the evolution of mitochondria. *Proceedings of the National Academy of Sciences of the United States of America* **2018**, *115*, 11796–11801.

(24) Lau, Y. H.; Giessen, T. W.; Altenburg, W. J.; Silver, P. A. Prokaryotic nanocompartments form synthetic organelles in a eukaryote. *Nature Communications* **2018**, *9*.

(25) Shevchenko, V. et al. Inward H+ pump xenorhodopsin: Mechanism and alternative optogenetic approach. *Science Advances* **2017**, *3*, e1603187.

(26) Inoue, K.; Ito, S.; Kato, Y.; Nomura, Y.; Shibata, M.; Uchihashi, T.; Tsunoda, S. P.; Kandori, H. A natural light-driven inward proton pump. *Nature Communications* **2016**, *7*, 13415.

(27) Marušič, N.; Otrin, L.; Zhao, Z.; Lira, R. B.; Kyrilis, F. L.; Hamdi, F.; Kastritis, P. L.; Vidaković-Koch, T.; Ivanov, I.; Sundmacher, K.; Dimova, R. Constructing artificial res-

piratory chain in polymer compartments: Insights into the interplay betweenbo3oxidase and the membrane. *Proceedings of the National Academy of Sciences* **2020**, *117*, 15006–15017.

(28) Goers, R.; Thoma, J.; Ritzmann, N.; Silvestro, A. D.; Alter, C.; Gunkel-Grabole, G.; Fotiadis, D.; Müller, D. J.; Meier, W. Optimized reconstitution of membrane proteins into synthetic membranes. *Communications Chemistry* **2018**, *1*.

(29) Kano, K.; Fendler, J. H. Pyranine as a sensitive pH probe for liposome interiors and surfaces. pH gradients across phospholipid vesicles. *Biochimica et Biophysica Acta (BBA) - Biomembranes* **1978**, *509*, 289–299.

(30) Langecker, M.; Arnaut, V.; Martin, T. G.; List, J.; Renner, S.; Mayer, M.; Dietz, H.; Simmel, F. C. Synthetic Lipid Membrane Channels Formed by Designed DNA Nanostructures. *Science* **2012**, *338*, 932–6.

(31) Göpfrich, K.; Li, C.-Y.; Ricci, M.; Bhamidimarri, S.; Yoo, J.; Gyenes, B.; Ohmann, A.; Winterhalter, M.; Aksimentiev, A.; Keyser, U. Large-Conductance Transmembrane Porin Made from DNA Origami. *ACS Nano* **2016**, *10*.

(32) Czogalla, A.; Kauert, D. J.; Franquelim, H. G.; Uzunova, V.; Zhang, Y.; Seidel, R.; Schwille, P. Amphipathic DNA Origami Nanoparticles to Scaffold and Deform Lipid Membrane Vesicles. *Angewandte Chemie International Edition* **2015**, *54*, 6501–5.

(33) Franquelim, H. G.; Khmelinskaia, A.; Sobczak, J.-P.; Dietz, H.; Schwille, P. Membrane sculpting by curved DNA origami scaffolds. *Nature Communications* **2018**, *9*, 811.

(34) Göpfrich, K.; Zettl, T.; Meijering, A. E. C.; Hernández-Ainsa, S.; Kocabey, S.; Liedl, T.; Keyser, U. F. DNA-tile structures lead to ionic currents through lipid membranes. *Nano Letters* **2015**, *15*, 3134–3138.

(35) Franquelim, H. G.; Dietz, H.; Schwille, P. Reversible membrane deformations by straight DNA origami filaments. *Soft Matter* **2020**,

(36) Green, L.; Amodio, A.; Subramanian, H. K. K.; Ricci, F.; Franco, E. pH-driven reversible self-assembly of micron-scale DNA scaffolds. *Nano Letters* **2017**, *17*, 7283–7288.

(37) Göpfrich, K.; Urban, M. J.; Frey, C.; Platzman, I.; Spatz, J. P. Dynamic Actuation of DNA-Assembled Plasmonic Nanostructures in Microfluidic Cell-Sized Compartments. *Nano Letters* **2020**, *20*, 1571–1577.

(38) Kuzyk, A.; Urban, M. J.; Idili, A.; Ricci, F.; Liu, N. Selective control of reconfigurable chiral plasmonic metamolecules. *Science Advances* **2017**, *3*, e1602803.

(39) Jahnke, K.; Weiss, M.; Frey, C.; Antona, S.; Janiesch, J.-W.; Platzman, I.; Göpfrich, K.; Spatz, J. P. Programmable Functionalization of Surfactant-Stabilized Microfluidic Droplets via DNA-Tags. *Advanced Functional Materials* **2019**, *29*, 1808647.

(40) Jia, H.-R.; Zhu, Y.-X.; Chen, Z.; Wu, F.-G. Cholesterol-Assisted Bacterial Cell Surface Engineering for Photodynamic Inactivation of Gram-Positive and Gram-Negative Bacteria. *ACS Applied Materials & Interfaces* **2017**, *9*, 15943–15951.

(41) Kilchherr, F.; Wachauf, C.; Pelz, B.; Rief, M.; Zacharias, M. H.; Dietz, H. Single-molecule dissection of stacking forces in DNA. *Science* **2016**, *353*, aaf5508.

(42) Vogel, S. K.; Wölfer, C.; Ramirez-Diaz, D. A.; Flassig, R. J.; Sundmacher, K.; Schwille, P. Symmetry Breaking and Emergence of Directional Flows in Minimal Actomyosin Cortices. *Cells* **2020**, *9*, 1432.

(43) Baumann, K. N.; Piantanida, L.; Garc, J.; Sobota, D.; Voitchovsky, K.; Knowles, T. P. J.; Hernandez-Ainsa, S. Coating and Stabilization of Liposomes by Clathrin-Inspired DNA Self-Assembly. *ACS Nano* **2020**, *14*, 2316–2323.

(44) Göpfrich, K.; Haller, B.; Staufer, O.; Dreher, Y.; Mersdorf, U.; Platzman, I.; Spatz, J. P. One-Pot Assembly of Complex Giant Unilamellar Vesicle-Based Synthetic Cells. *ACS Synthetic Biology* **2019**, *8*, 937–947.

(45) Kopperger, E.; List, J.; Madhira, S.; Rothfischer, F.; Lamb, D. C.; Simmel, F. C. A self-assembled nanoscale robotic arm controlled by electric fields. *Science* **2018**, *359*, 296–301.

(46) Douglas, S. M.; Marblestone, A. H.; Teerapittayanon, S.; Vazquez, A.; Church, G. M.; Shih, W. M. Rapid prototyping of 3D DNA-origami shapes with caDNAno. *Nucleic acids research* **2009**, *37*, 5001–5006.

(47) Zheng, S. Q.; Palovcak, E.; Armache, J.-P.; Verba, K. A.; Cheng, Y.; Agard, D. A. MotionCor2: anisotropic correction of beam-induced motion for improved cryo-electron microscopy. *Nature Methods* **2017**, *14*, 331–332.

(48) Schindelin, J. et al. Fiji: an open-source platform for biological-image analysis. *Nature Methods* **2012**, *9*, 676–682.

Figures

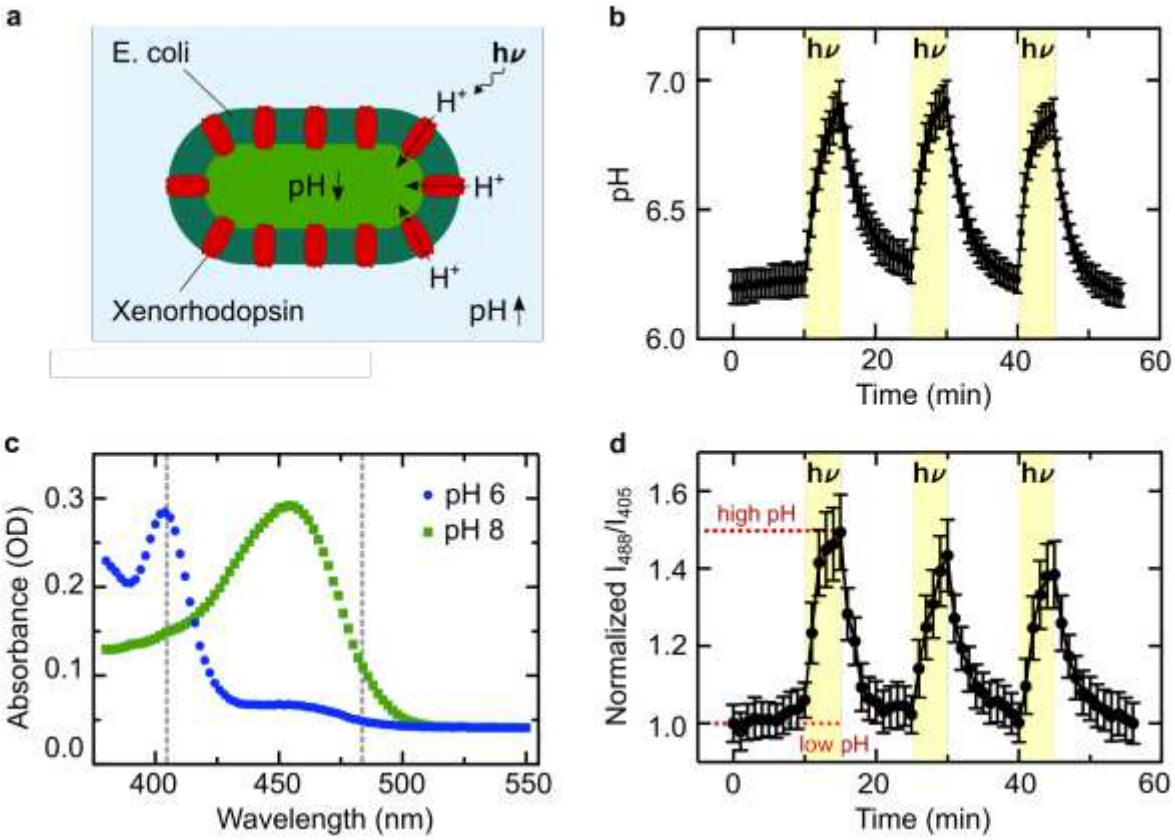

Figure 1

Genetically engineered xenorhodopsin-expressing E. coli generate a pH gradient upon illumination with white light. a Schematic illustration of an E. coli expressing xenorhodopsin, a light-driven proton pump (red), allowing for the reversible generation of a directional pH gradient during illumination with white light. The inward pump increases the pH of the external solution. b Photoactivity generated by the E. coli (OD600=20, in 150 mM NaCl) measured with an external pH electrode. The pH is plotted over time during three light-dark cycles (periods of illumination are indicated in yellow). The pH increases by almost one pH unit within 5 min of illumination and nearly returns to its original value after 10 min in the dark (mean±s.d., n=3). c Absorbance measurements of the pH-sensitive ratiometric fluorophore pyranine at pH 6 (blue) and pH 8 (green). The pH can be quantified as the fluorescence intensity ratio at the excitation wavelengths 488 nm and 405 nm (gray dashed lines). d Normalized fluorescence intensity ratio I488/I405 of pyranine (50 μM) over time in a solution containing E. coli and lipid vesicles as determined with confocal fluorescence microscopy (mean±s.d., n=4). Periods of illumination are indicated in yellow.

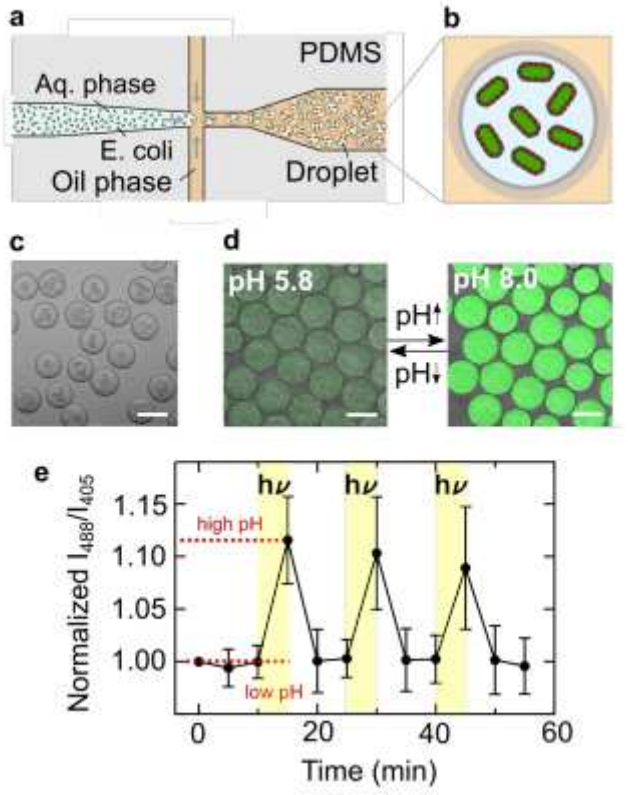

Figure 2

Using E. coli as light-activated synthetic organelles that change the pH inside cellsized confinement. a Schematic illustration of the microfluidic device used to encapsulate engineered E. coli and pyranine into cell-sized compartments. Water-in-oil droplets were generated at a flow-focusing T-junction of a PDMS-based device. b Schematic illustration of a surfactant-stabilized water-in-oil droplet containing engineered E. coli. c Brightfield image of monodisperse water-in-oil droplets with a radius of 27±5 µm (mean±s.d., n=53) containing engineered E. coli (OD600 = 20). Scale bar: 50 µm. d Overlay of confocal fluorescence and brightfield images of pyranine (c= 50 µM, λex=488 nm) inside droplet-based compartments at pH 5.8 and pH 8.0. Scale bar: 50 µm. e Normalized fluorescence intensity ratio I488/I405 of E. coli and pyranine-containing droplets over time. The fluorescence intensity ratio (mean±s.d., n=11 droplets) of pyranine (and hence the pH) increases reversibly during periods of illumination with white light (30W halogen bulb, highlighted in yellow). Note that the number of recorded frames was reduced because the illumination light had to be turned off each time an image was acquired, which will bias the proton pumping activity.

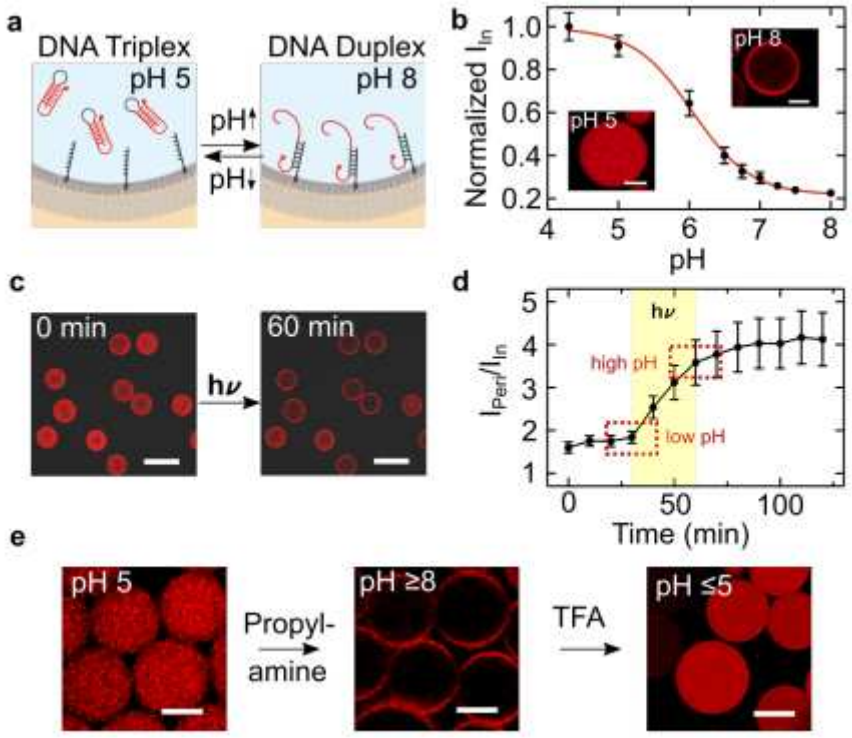

Figure 3

pH-sensitive DNA attachment to the droplet periphery stimulated with engineered E. coli. a Schematic illustration of pH-sensitive duplex formation at the droplet periphery. In response to higher pH, the DNA triplex motif opens up and reversibly attaches to the cholesterol-tagged DNA handles at the compartment periphery. b Normalized fluorescence intensity of triplex-forming DNA inside the droplet (excluding the periphery) dependent on the pH (mean±s.d., n=20). The sigmoidal fit (red curve) has a turning point at pH 6.05. The insets depict confocal fluorescence images of Cy5-labeled triplex-forming DNA (λex=647 nm, 1 μM) inside a water-in-oil droplet (containing 1.5 μM cholesterol-tagged DNA) at pH 5 (bottom left) and pH 8 (top right). At pH 8, the triplex-forming DNA is located at the droplet periphery, whereas it is homogeneously distributed at pH 5. Scale bars: 20 μm. c Confocal images of microfluidic water-in-oil droplets containing the triplex-forming DNA (λex=647 nm), cholesterol-tagged DNA and engineered E. coli before (0 min) and after (60 min) illumination with white light. Scale bars: 100 μm. d Fluorescence intensity ratio Iperi/Iin (mean±s.d., n=20) of the triplex-forming DNA over time. The ratio increases during light illumination due to binding of the triplex-forming DNA to the droplet periphery. The time period of illumination is indicated in yellow. e Confocal images of microfluidic water-inoil droplets containing the triplex-forming DNA (λex=647 nm) and cholesterol-tagged DNA produced at pH 5 (left image). Flushing of the proton acceptor propylamine (1 vol% in HFE) led to a pH increase of the aqueous solution inside the droplets and hence attachment of the triplex-forming DNA (middle). Subsequent flushing of the proton donor trifluoroacetic acid (1 vol% in HFE) decreased the pH and hence causes DNA detachment (right). The attachment of triplex-forming DNA to the droplet periphery is reversible. Scale bars: 30 μm.

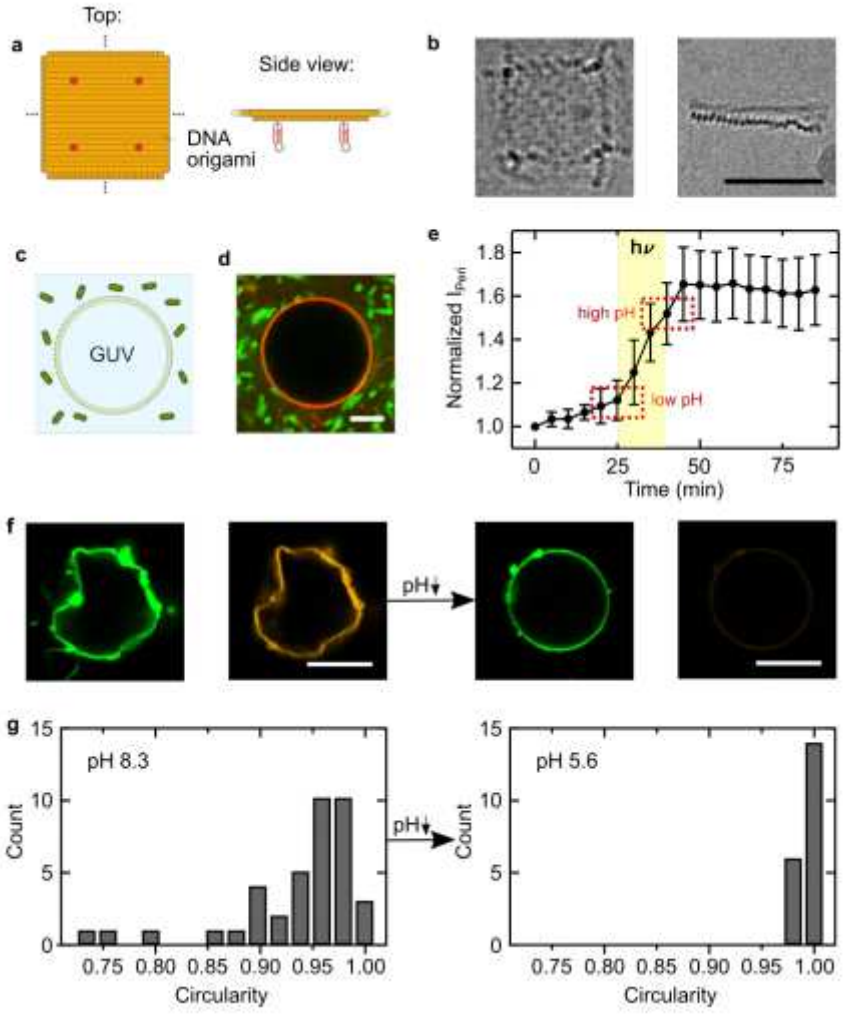

Figure 4

Deformation of GUVs with pH-sensitive DNA origami. a Schematic illustration of the DNA origami, which can polymerize into flat DNA origami sheets due to blunt end stacking. The DNA origami was functionalized with four DNA triplex motifs (red, two are shown), such that its assembly on the GUV membrane is pH-dependent.b Cryo-EM micrographs of the DNA origami plates. The top view (left) and the side view (right) showing the two DNA layers connected at a 90□ angle. Scale bar: 50 nm. c Schematic illustration of a GUV immersed in a bath of engineered E. coli. d Confocal image of a DNA-coated GUV surrounded by E. coli as described in a (0.4 μM triplex-forming DNA, λex=561 nm; 0.6 μM cholesterol-tagged DNA). Scale bar: 10 μm. e Normalized fluorescence intensity Iperi (mean±s.d., n=15) of the triplexforming DNA at the GUV periphery monitored over time. The time period of illumination is indicated in yellow, illumination leads to a pH increase and hence DNA attachment. f Confocal images of GUVs before (left) and after (right) decreasing the pH from pH 8.3 to pH 5.6 by addition of iso-osmotic potassium dihydrogenphosphate buffer. The GUV (lipids labelled with Atto488, λex= 488 nm) is initially deformed due to the membrane-bound polymerized DNA origami (labelled with Cy3, λex= 561 nm). The DNA origami detaches upon lowering the pH (the fluorescence from the detached DNA origami in the background is too weak to be visible). Scale bars: 10 μm. g Histograms of GUV circularity before (left)

and after (right) lowering the pH. At pH 8.3, the mean circularity is 0.94 ± 0.06 (n=39) compared to 0.991 ± 0.004 (n=20) at pH 5.6, respectively.

Supplementary Files

This is a list of supplementary files associated with this preprint. Click to download.

- VideoS1.avi
- VideoS2.avi
- VideoS3.mp4
- VideoS4.avi
- VideoS5.avi
- SIJahnke.pdf